Journal Pre-proof

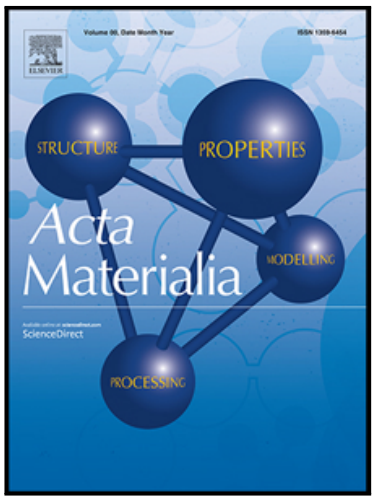

Violation of the Stokes-Einstein relation in $Ge_2Sb_2Te_5$, GeTe, $Ag_4In_3Sb_{67}Te_{26}$, and $Ge_{15}Sb_{85}$, and its connection to fast crystallization

Shuai Wei , Christoph Persch , Moritz Stolpe , Zach Evenson , Garrett Coleman , Pierre Lucas , Matthias Wuttig

PII: S1359-6454(20)30391-8
DOI: https://doi.org/10.1016/j.actamat.2020.05.044
Reference: AM 16054

To appear in: *Acta Materialia*

Received date: 4 May 2020
Accepted date: 17 May 2020

Please cite this article as: Shuai Wei , Christoph Persch , Moritz Stolpe , Zach Evenson , Garrett Coleman , Pierre Lucas , Matthias Wuttig , Violation of the Stokes-Einstein relation in $Ge_2Sb_2Te_5$, GeTe, $Ag_4In_3Sb_{67}Te_{26}$, and $Ge_{15}Sb_{85}$, and its connection to fast crystallization, *Acta Materialia* (2020), doi: https://doi.org/10.1016/j.actamat.2020.05.044

Violation of the Stokes-Einstein relation in $Ge_2Sb_2Te_5$, GeTe, $Ag_4In_3Sb_{67}Te_{26}$, and $Ge_{15}Sb_{85}$, and its connection to fast crystallization

Shuai Wei[a*], Christoph Persch[a], Moritz Stolpe[b], Zach Evenson[c], Garrett Coleman[d], Pierre Lucas[d], and Matthias Wuttig[a,e*]

a. Institute of Physics (IA), RWTH Aachen University, 52074 Aachen, Germany
b. Heraeus Holding GmbH, Heraeusstraße 12-14. 63450, Hanau, Germany
c. Maier-Leibnitz Zentrum (MLZ) and Physik Department, Technische Universität München, Lichtenbergstrasse 1, 85747 Garching, Germany
d. Department of Materials Science and Engineering, University of Arizona, Tucson, Arizona 85712, United States.
e. JARA-Institute Green IT (PGI-10), FZ-Jülich, 52428 Jülich, Germany

ABSTRACT: Phase-change materials (PCMs) are already commercialized in optical and non-volatile memory devices. Yet, the dynamics of atomic rearrangement processes and their temperature dependence, which govern their ultrafast switching, are still not fully understood. Here we use quasi-elastic neutron scattering to investigate the liquid-state dynamics of four prevailing PCMs $Ge_2Sb_2Te_5$, GeTe, $Ag_4In_3Sb_{67}Te_{26}$(AIST), and $Ge_{15}Sb_{85}$ above their respective melting points T_m. Self-diffusion coefficients and structural relaxation times on the timescale of picoseconds are extracted from dynamic structure factors. The results indicate an unusual systematic violation of the Stokes-Einstein relation (SER) for each PCM in high-temperature regions above T_m, where the atomic-mobility is high. This is likely related to the formation of locally favored structures in liquid PCMs. Absolute values of diffusivity in the supercooled liquid AIST are derived from crystal-growth velocity, which are almost one order of magnitude higher than that expected from the SER in the technologically relevant temperature range ~20% below T_m. This is relevant to understand the crystallization kinetics of PCMs as crystal growth is controlled by diffusivity. Furthermore, the instantaneous shear modulus is determined ranging from 2 to 3 GPa for liquid PCMs, which permits extracting viscosity from microscopic structural relaxations usually accessible to simulations and scattering techniques.

*shuai.wei@physik.rwth-aachen.de, +49 241-80-27169 (S.W.); wuttig@physik.rwth-aachen.de, +49 241 80 27155 (M.W.).

Keywords: phase-change materials; structural relaxation; viscosity; diffusion; crystallization

1. Introduction

Phase-change materials (PCMs) such as Ge-Sb-Te, GeTe, Ag-In-Sb-Te, and $Ge_{15}Sb_{85}$ alloys can be rapidly and reversibly switched between amorphous and crystalline states on a timescale of nanoseconds[1–3,3,4] or even picoseconds[5]. Thanks to the unique combination of ultrafast switching, strong electrical/optical contrast, and a relatively stable amorphous state, these PCMs have been identified as the most viable candidates for the development of commercial non-volatile computer memory technologies[2,3,6–8]. Microelectronic industry leaders such as Intel and Micron have already commercialized phase-change memory devices such as 3D XPoint memory[9]. In addition, IBM has developed PCM-based devices that mimic neuronal functions for neuromorphic computing[10]. Yet, despite these commercial successes, several fundamental aspects of PCMs remain poorly understood, in particular regarding the temperature dependence of the kinetic properties that elicits their ultrafast switching capabilities.

The structure-bonding-property relationship of crystalline PCMs has been the subject of extensive studies[2,11,12]. Crystalline PCMs possess a unique bonding mechanism – coined metavalent bonding[3,13]. This bonding is characterized by a competition between electron localization and delocalization[14]. This competition either leads to Peierls-like distortions or to charge transfer between adjacent atoms, creating a distinct "island" of physical properties between metallic, covalent and ionic regimes[3,7]. Hence, they represent a class of "incipient metals"[3]. On the other hand, the amorphous phase of PCMs is a covalently bonded semiconducting solid. Most covalent glasses (such as SiO_2) fit into Zachariasen's glass picture[15], where the local atomic arrangement in the glass resembles that in the crystalline state, but lacks long-range order. By contrast, amorphous PCMs deviate from Zachariasen's glass picture[1,15]. During the switching processes, the amorphous solid ('off-state'), rapidly heated by an electrical or optical pulse, can be transformed into the supercooled liquid before rapid crystallization ('on-state'). To switch back to the "off-state", the crystalline phase is molten into liquid by a larger pulse before quenching into the amorphous (glassy) solid. Hence, the liquid state plays an essential role in both the 'on' and 'off' switch. According to the classical crystallization theory, the kinetic factor for both

nucleation and growth depends on the atomic mobility of the liquid[16,17]. Therefore, the kinetic properties of this state play an important role in the crystallization kinetics and fast switching behaviors[18–20].

The atomic mobility of the liquid can be characterized by diffusivities, viscosities, and structural relaxation times. However, the measurement of these properties below T_m (i.e. supercooled liquid) is a long-standing experimental challenge for PCMs due to the interference of fast crystallization. PCMs are very poor glass formers with T_g/T_m~0.5[21,22]. Hence, they require critical cooling rates of ~10^9 K s^{-1} for vitrification[23]. Previously, the temperature dependence of viscosity has been estimated using an indirect approach involving a derivation of the liquid kinetics from crystallization rates. In these studies, the Stokes-Einstein relation (SER), has been broadly used to connect viscosity η to diffusivity D according to:

$$D\eta = \frac{k_B T}{6\pi r_H} \tag{1}$$

where k_B is the Boltzmann constant, T the absolute temperature, and r_H the effective hydrodynamic radius. The SER is usually assumed to be valid at least at high temperatures above T_m (ref.[18,19,24–26]), although it is known to break down in the viscous regime of deeply supercooled liquids around ~$1.2T_g$ (ref.[27,28]), as demonstrated by AIMD simulations in the supercooled liquid PCM GeTe [29]. The breakdown of SER near T_g is believed to result from the emergence of dynamic spatial heterogeneities[27,30]. Nevertheless, a recent experimental study of $GeSb_2Te_4$ has shown that the SER can break down at much higher temperature even above T_m where the high fluidity state exhibits relaxation on a picosecond time scale[20]. The origin of the breakdown has been discussed in the context of thermodynamic anomalies in liquids and linked to similar phenomena observed in liquid silicon, germanium and supercooled water[20]. The questions arise whether the SER breakdown in such a high fluidity state is a general phenomenon in PCMs, and if it precedes any kind of anomalies, such as a liquid-liquid transition (LLT) in the supercooled liquid state as suggested earlier[31]. Testing the SER in PCM melts requires simultaneous measurements of the diffusivity D and the structural relaxation time τ_a (to derive the viscosity η). Both measurements can be performed by quasi-elastic neutron scattering (QENS).

In addition, direct measurement of diffusivities above T_m provides the reference values necessary to use crystal growth velocities to derive a wide range of diffusivities in a temperature range inaccessible to conventional experimental techniques. Such an approach has been successfully employed to obtain the diffusivity of supercooled water [32]. The diffusivity data in this regime can provide a quantitative measure of the departure from the SER behavior down to the deeply supercooled state. This is of particular interest since diffusivity is the most fundamental parameter for understanding crystallization kinetics[33]. Yet its contribution is generally less discussed than that of viscosity.

Finally, measurements of the structural relaxation time τ_α provide a mean of investigating the non-trivial relation between relaxation time and viscosity in liquid PCMs. The characteristic timescale τ_α of liquids is commonly derived from computer simulations, calorimetric, or QENS studies; while the viscosity η is a macroscopic measure of internal friction of a fluid, usually measured by viscometers. According to the generalized Maxwell viscoelastic model, the stress relaxation time τ_s is proportional to η (Maxwell relation)[34],

$$\eta = G_\infty \tau_s, \tag{2}$$

where G_∞ is the instantaneous shear modulus and τ_s is usually interchangeable with structural relaxation time τ_α in the literature[35–37]. G_∞ is usually assumed to be weakly temperature dependent. However, no experimental data of the temperature dependence of G_∞ is available for PCMs and the validity of Eq. (2) has not been tested in PCMs.

2. Experimental Methods

Samples preparation

$Ge_2Sb_2Te_5$, GeTe, AIST and $Ge_{15}Sb_{85}$ samples were prepared using the Ge, Sb, Ag, In, and Te elements with purities ranging from 99.999 to 99.9999 at. %. The elements were sealed under vacuum (10^{-6} mbar) in a fused quartz tube with internal diameter of 5 mm designed for loading into Al_2O_3 cylinders for QENS measurements and synthesized in a rocking furnace for homogenization at 900°C for 15 hours.

Quasi-elastic neutron scattering

The QENS experiments allow measurement of the dynamic structure factor $S(q, \omega)$, where q is the momentum transfer and $\hbar\omega$ is the energy transfer. By determining the half-width at half maximum (HWHM) of the quasi-elastic broadening observed in $S(q, \omega)$, Γ, we obtain a relaxation time τ via $\Gamma = \hbar/\tau$. At the first structure factor maximum q_0, the QENS signal is dominated by coherent scattering contributions, which is a weighted average of the corresponding coherent neutron scattering cross-section of the constituents (Table S1) and their concentrations in the sample. Thus, the relaxation time τ derived at q_0 (q_0=2.0 Å^{-1} for $Ge_2Sb_2Te_5$, q_0=2.1 Å^{-1} for AIST, q_0=2.1 Å^{-1} for $Ge_{15}Sb_{85}$ and q_0=2.0 Å^{-1} for GeTe) reflects the collective atomic motions and corresponds to a characteristic timescale of structural relaxations, τ_α [38,39].

The QENS measurements were performed on the time-of-flight spectrometer (TOFTOF) at the neutron source Heinz Meier-Leibnitz (FRM II) in Munich, Germany[40,41]. It is worth emphasizing that since the samples were always sealed in fused quartz tubes, prior to being loaded in thin-walled (1 mm) Al_2O_3 cylinders, there were no evaporation issues leading to possible changes in sample compositions. Post-mortem inspection of the samples and in-situ observation of a constant neutron count profile as a function of isothermal holding time confirmed no breakage of the quartz tubes and subsequent evaporation of the molten samples. The measurements were carried out in a high-temperature Nb furnace using an incident neutron wavelength of λ = 5.1 Å, yielding an accessible momentum transfer range 0.4 Å^{-1} < q < 2.6 Å^{-1} at zero energy transfer and an instrumental energy resolution of about 100 μeV (full width at half maximum). The measured scattered intensities as functions of scattering angle and the neutron flight time, $I(2\theta, tof)$, were converted to the dynamic structure factor $S(q,\omega)$ after appropriate corrections such as normalization to a vanadium standard, correction for self-absorption, interpolation to constant q, and symmetrizing with respect to energy with the detailed balance factor using the Mantid software[42]. All spectra were fitted with a composite function convoluted with the instrumental resolution,

$$S(q,\omega) = R(q,\omega) \otimes N\left[A_0\delta(\omega) + (1 - A_0)L(q,\omega)\right] + b(q,\omega), \quad (3)$$

where $R(q,\omega)$ is the instrumental resolution function, N is a normalization factor, A_0 is the magnitude of the elastic scattering, a delta-function to take care of any elastic scattering emanating from the sample

holder, and $b(q,\omega)$ is a constant but q-dependent, background. The symbol $\otimes$ denotes a numerical convolution. The quasi-elastic broadening was found to be best described with a single Lorentzian of the form (see Fig.1),

$$L(q,\omega) = \frac{1}{\pi}\frac{\Gamma(q)}{(\hbar\omega)^2 + \Gamma(q)^2}, \tag{4}$$

where Γ is the half-width at half-maximum (HWHM). We restricted the fitting range in the energy transfer domain to $[\hbar\omega_1, \hbar\omega_2]$, where $\hbar\omega_1 \approx$ -2.5 meV and $\hbar\omega_2 \approx$ 0.8–1.8 meV depending on the data availability of materials on the positive energy transfer. At higher energy transfers, the spectra are dominated by phononic vibrations and fast relaxation processes.

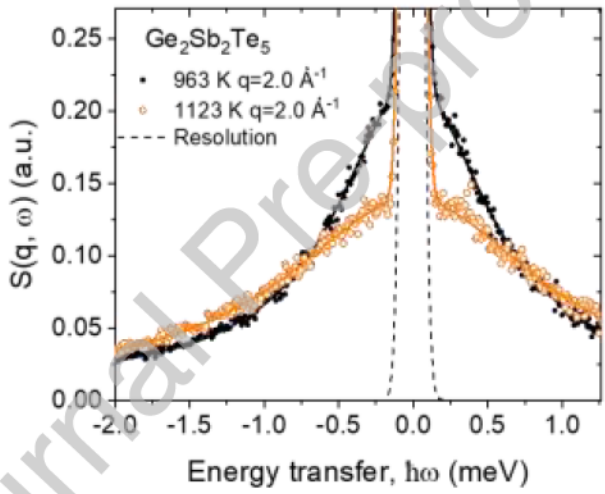

Figure 1. Dynamic structure factor $S(q, \omega)$ at q=2.0 Å^{-1} for 963 K and for 1123 K for $Ge_2Sb_2Te_5$. Lines are fits with a Lorentzian function convoluted with the energy resolution function and linear background (Eq. 3). The dashed line represents the resolution function.

3. Results

Quasi-elastic neutron scattering (QENS) probes atomic dynamics on a microscopic level. The dynamic structure factors $S(q, \omega)$ of liquid PCMs shown in Fig.2a, consist of a coherent and an incoherent scattering contribution. While the coherent contribution reflects collective motion of atoms, the incoherent contribution depicts single particle motions. At the momentum transfer q_0 of the first structure factor maximum when the QENS signal is dominated by coherent scattering

contributions[38,39], a characteristic timescale of structural relaxations τ_α can be determined by fitting the $S(q_0, \omega)$ data, $\tau_\alpha=\hbar/\Gamma$, where Γ is half width at half maximum (HWHM), as shown in Fig. 2b (see Sec. 2 for Methods). A Fourier transform of $S(q_0, \omega)$ in the frequency domain yields an intermediate scattering function which describes the rate of microscopic density fluctuations in the liquid, caused by collective atomic motions[38]. Thus, τ_α is a measure of the rate of decay of intermediate scattering functions. It is proportional to the macroscopic shear viscosity, via the Maxwell relation (Eq.2).

At the low-q range, incoherent contributions dominate the scattering signal (Fig.2c), reflecting long-range single atomic diffusion. Therefore, the self-diffusivity D can be determined from the broadness of incoherent scattering dynamic structure factor[43,44] (see Sec.3.2 for details). Hence, structural relaxation time τ_α and diffusivity D can be determined for each temperature.

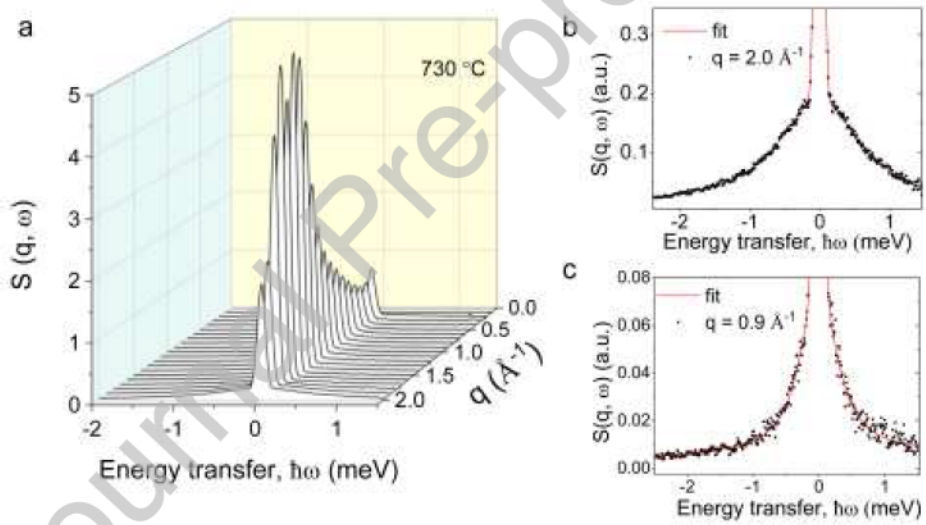

Figure 2. Example of dynamic structure factors $S(q, \omega)$ of $Ge_2Sb_2Te_5$ measured by quasi-elastic neutron scattering (QENS) at 730°C. (**a**) $S(q, \omega)$ as a function of energy transfer $\hbar\omega$ and momentum transfer q. (**b**) Example of the coherent scattering at the characteristic length scale at the first structure factor maximum q_0=2.0 Å^{-1} to determine the structural relaxation time τ_α. (**c**) Example of the incoherent scattering at low-q to obtain the diffusivity D. The fits yield the relaxation time τ_α (b) and τ_{inc} (c), respectively (see Methods).

3.1. α-relaxation times

Figure 3 shows τ_α for liquid $Ge_2Sb_2Te_5$ above its liquidus temperature T_l=911 K (T_m=894 K), for AIST above its T_l=817 K (T_m=810 K)[21], for $Ge_{15}Sb_{85}$ above its eutectic melting T_m=865 K[45], and for GeTe above its T_m=997 K[46]. The τ_α of $Ge_2Sb_2Te_5$ is slightly lower than that of GeTe, indicating that liquid $Ge_2Sb_2Te_5$ has faster relaxation dynamics than GeTe. The τ_α of AIST and $Ge_{15}Sb_{85}$ are markedly lower than that of both $Ge_2Sb_2Te_5$ and GeTe alloys. Hence, the Sb-rich alloys AIST and $Ge_{15}Sb_{85}$ have faster collective atomic motions compared to those of $Ge_2Sb_2Te_5$ and GeTe alloys in the equilibrium

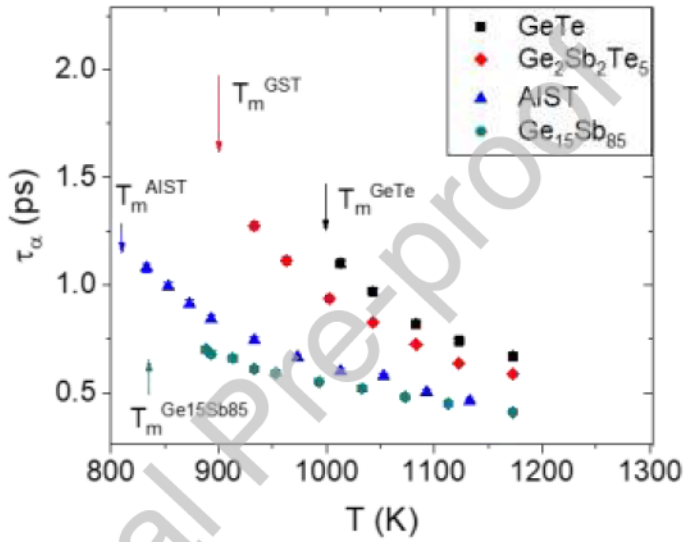

melts above their T_m.

Figure 3. α-relaxation times τ_α determined from QENS at the first structure factor maximum q_0 for PCMs. T_m indicates the melting temperature for AIST (T_m=810 K), $Ge_2Sb_2Te_5$ (T_m=894 K), $Ge_{15}Sb_{85}$ (T_m=865 K), and GeTe (T_m=997 K). Error bars indicate the standard deviation.

3.2. Self-diffusivity

The dynamics of single particle motion in a liquid is described by the self-correlation function $G_s(r, t)$ that gives correlation information of a tagged particle between two space-time points. In the long-wavelength λ fluctuations, the self-correlation function $G_s(r, t)$ behaves as if the tagged single particle were undergoing simple diffusion[47]. This is the hydrodynamic limit of $G_s(r, t)$, i.e. $\lambda \rightarrow \infty$ and $q = 2\pi/\lambda$

→ 0. In this limit, $G_s(r, t)$ is dominated by the diffusion equation and related to the self-diffusivity D via [(Eq. 4.3.7) of ref.[47]]

$$\frac{\partial}{\partial t} G_s(r,t) = -D\nabla^2 G_s(r,t) \tag{5}$$

In experiments, $G_s(r, t)$ is the Fourier Transforms of the incoherent (i.e. single particle) dynamic structure factor $S_{inc}(q, \omega)$, which is described by a single central Lorentzian form. Thus, $S_{inc}(q, \omega)$ is related to D given by Boon and Yip [(Eq. 4.3.10) of ref.[47]]

$$S_{inc}(q,\omega) = \frac{1}{\pi}\frac{Dq^2}{\omega^2+(Dq^2)^2} \tag{6}$$

Then, the HWHM of $S_{inc}(q, \omega)$ for the diffusion model is $\Gamma = Dq^2$[ref.[47]]. Note that in practical data treatments, frequency ω in the x-axis is usually plotted as energy transfer $\hbar\omega$, as for our case. Then the HWHM is $\Gamma = \hbar Dq^2$.

In the low-q range where the model applies, Γ should be proportional to q^2 and the coefficient D is a constant. Thus, the self-diffusion coefficients D can be determined from the QENS signal at low q-values (Fig.4a), where the signal is dominated by incoherent scattering (see SI for a detailed consideration). In this q range, the measured broadening of incoherent Γ follows $\Gamma \propto q^2$, as shown in Fig.4b-e. The self-diffusion coefficient D can thus be derived by a fit of $D = \Gamma/(\hbar q^2)$(ref.[43,44]) with a

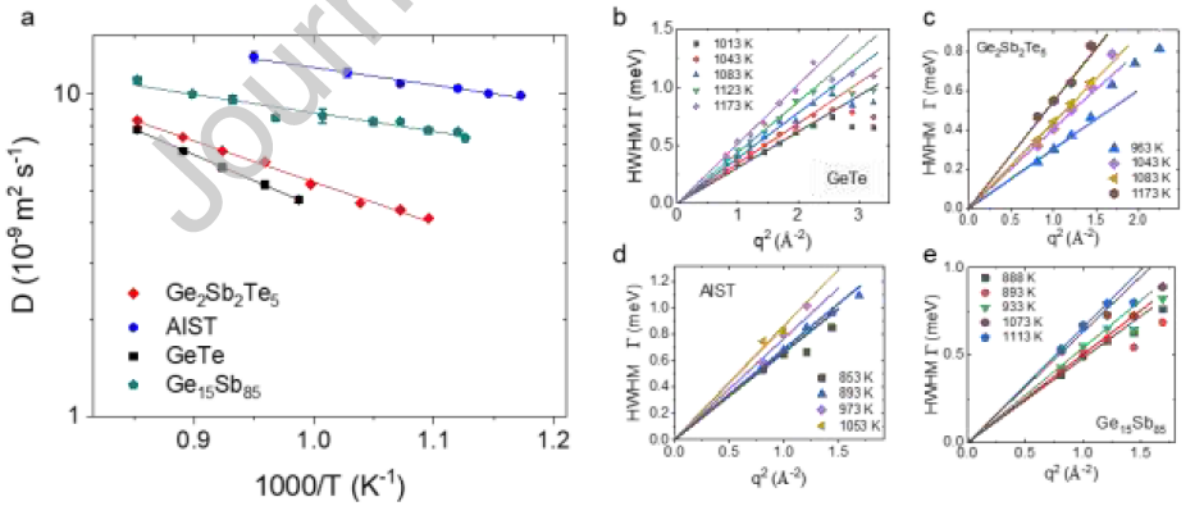

fixed (0,0) point.

Figure 4. (a) Mean self-diffusion coefficients D of $Ge_2Sb_2Te_5$, GeTe, AIST, and $Ge_{15}Sb_{85}$ above their respective T_m derived from the incoherent scattering at low-q. Error bars indicate the standard deviation. The HWHM $\Gamma=\hbar/\tau^{inc}$ is proportional to q^2 at low-q range for (b) GeTe ($q^2 \leq$ 2.3 Å^{-2}), (c) $Ge_2Sb_2Te_5$ ($q^2 \leq 1.2$ Å^{-2}), (d) AIST ($q^2 \leq 1.0$ Å^{-2}), and (e) $Ge_{15}Sb_{85}$ ($q^2 < 1.3$ Å^{-2}). At large q, a deviation from the linear fit is observed, which is similar to that reported for $GeSb_2Te_4$[20].

Figure 4a shows the mean self-diffusion coefficients D for $Ge_2Sb_2Te_5$, GeTe, AIST, and $Ge_{15}Sb_{85}$, which are weighted by incoherent atomic scattering cross sections and atomic fractions of the respective alloys. The incoherent atomic scattering cross-sections of the constituents can be found in the NIST standard table (Table S1), 0.18 barn for Ge, 0.09 barn for Te, 0.007 barn for Sb, 0.58 barn for Ag, and 0.54 barn for In. Since the incoherent cross-section of Sb is more than 10 times smaller than those of Ge and Te, the signals are primarily caused by the Ge- and/or Te-constituents of the alloys. The Ge/Te-content constitutes a significant fraction for GeTe (100%) and $Ge_2Sb_2Te_5$ (78%), whereas, for $Ag_4In_3Sb_{67}Te_{26}$ (AIST), the Te-content constitutes only 26%, and the constituents (i.e. Ag and In), having a high incoherent scattering cross-section, are only used as dopants in a small concentration. The 67% Sb in AIST makes vanishingly small contributions due to its much smaller incoherent cross-section. As a consequence, only 1/3 of atoms in the sample of AIST effectively contribute to the incoherent scattering signals. Also taking into account the relatively greater neutron absorption cross-sections of both Ag and In, this leads to overall lower signal-to-noise ratios and, hence, more difficulties in fitting the $S(q, \omega)$ in the low-q range especially at high temperatures, where the amplitude of the quasielastic line lowers toward the order of the noise, such that a reasonable fit the data cannot be carried out. By contrast, the relaxation time τ_α is extracted from the coherent scattering signals at the first structure factor maximum q_0, where the larger coherent scattering cross-sections of elements (Table S1) allow for higher signal-to-noise ratios and data fitting at higher temperatures. Keeping these experimental limits in mind, the resulting diffusivity of AIST is of the order ~10^{-8} m^2 s^{-1}, being within a reasonable range, which is somewhat higher than the D values of 0.4-0.8 ×10^{-8} m^2 s^{-1} for both GeTe and $Ge_2Sb_2Te_5$. A simple Arrhenius fit $D=D_0 exp(E_{a,D}/RT)$ yields an activation energy of diffusivity, $E_{a,D}$= 10.4 ± 0.8 kJ mol^{-1} (≈ 0.11 eV/atom) for AIST, $E_{a,D}$= 24.5 ± 0.8 kJ mol^{-1} (≈ 0.25 eV/atom) for GST, and $E_{a,D}$= 30.7 ± 0.6 kJ mol^{-}

^{1} (≈ 0.32 eV/atom) for GeTe. For another Sb-rich alloy $Ge_{15}Sb_{85}$, Ge atoms dominate the incoherent contribution, and the diffusivity is slightly lower than that of AIST with an activation energy $E_{a,D}$= 11.0 ± 1.0 kJ mol^{-1} (≈ 0.11 eV/atom) nearly the same as that of AIST.

The atomic diffusive motion is faster in AIST and $Ge_{15}Sb_{85}$ than in $Ge_2Sb_2Te_5$ and GeTe. A similar comparison can be also noted for the collective atomic motion, where it is faster in the Sb-rich alloys than in $Ge_2Sb_2Te_5$ and GeTe, as reflected by $\tau_\alpha(Ge_{15}Sb_{85})<\tau_\alpha(AIST)<\tau_\alpha(GST)<\tau_\alpha(GeTe)$ shown in Figure 3. This is also consistent with the difference in their crystal growth velocities, where the value for melt-quenched AIST[18] is about two orders magnitude higher than that of melt-quenched $Ge_2Sb_2Te_5$[48] in the accessible temperature range (450 to 550 K).

4. Discussion

4.1. Stokes-Einstein relation with α-relaxation time and viscosity

The SER connects the viscosity η to diffusivity D through temperature and a series of constants. Therefore it is commonly rewritten in the form[37,49],

$$D\eta/T = \text{constant}. \tag{7a}$$

Since the proportionality between η and τ_α is usually assumed in the literature[36–38], the SER can also be rewritten in terms of τ_α as[37]

$$D\tau_\alpha/T = \text{constant}. \tag{7b}$$

An alternative relation between η and τ_α is proposed as $\tau_\alpha \propto \eta/T$ from the Gaussian solution to the diffusion equation[35,50]. With this form, the SER is rewritten as[35,51]

$$D\cdot\tau_\alpha = \text{constant}. \tag{7c}$$

If the SER holds, the product $D\eta/T$, $D\tau_\alpha/T$, or $D\cdot\tau_\alpha$ should be a temperature-independent constant, according to Equations 3a-c. Figure 5a shows the form $D\tau_\alpha/T$ (Eq. 7b) for $Ge_2Sb_2Te_5$, AIST, and GeTe normalized to their respective values at the highest temperatures measured. For comparison, all y-axes are plotted on the same scale. The values of $D\tau_\alpha/T$ are not constant, but increase with decreasing temperature, indicating a breakdown of the SER well above T_m. For $Ge_2Sb_2Te_5$, the deviation

begins around 1120 K and reaches about 1.5 times higher at about 903 K. The result is consistent with the previously reported breakdown of SER in $GeSb_2Te_4$.[20] For AIST, the increase in $D\tau_a/T$ is about a factor of 1.6, as the temperature decreases from 1050 K to 850 K; however, the data apparently do not show a plateau yet, as high-temperature data are not available due to the poor signal-to-noise ratio of the incoherent scattering. $Ge_{15}Sb_{85}$ exhibits a similar behavior without reaching a plateau in the accessible temperature range. The weakest deviation is observed in GeTe, which starts from about 1080 K and reaches about 1.2 times higher at about T_m=997 K.

In Figure 5b, we test the alternative form, Eq. 7c, of the SER. $D{\cdot}\tau_a$ behaves slightly differently from $D\tau_a/T$. The $D{\cdot}\tau_a$ of $Ge_2Sb_2Te_5$ deviates from unity at a lower temperature 1000 K. $D{\cdot}\tau_a$ of AIST and $Ge_{15}Sb_{85}$ seem to have reached a plateau at high temperatures. $D{\cdot}\tau_a$ of GeTe exhibits a small, but notable decrease in the ratio with decreasing temperature down to 1100 K, termed as a "negative violation" by Z. Shi et al.[35], before it increases again at lower temperatures. Such a minimum ("negative violation") in $D{\cdot}\tau_a$ has been also observed in model atomic systems with softened pair potentials using molecular

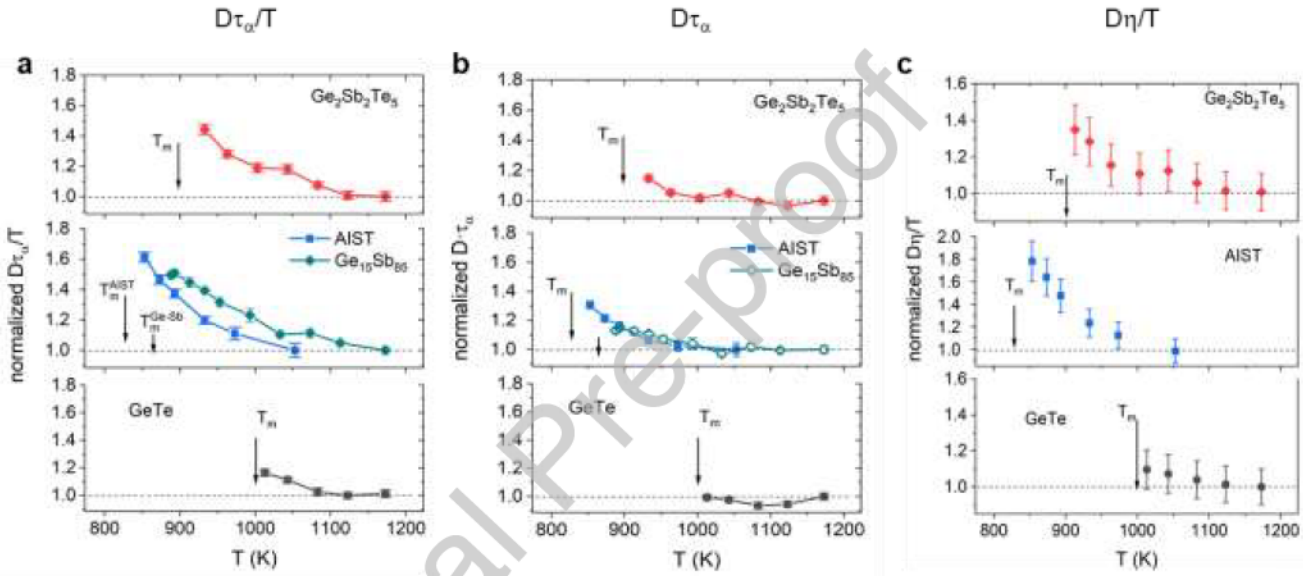

dynamic simulations[35]. However, such a negative violation was not observed in the molecular system of ortho-terphenyl (OTP), where $D{\cdot}\tau_a$ was also shown as a good substitute for the original SER ratio with viscosity η (i.e. Eq.7a). R. Shi et al.[52,53] showed that the SER in the form, $D{\cdot}\tau_a$ = constant, holds well at high temperatures in two water models before it breaks down at lower temperatures. In our case, $D\tau_a/T$ appears to be a better substitute for the original SER ratio (Eq.7a), as discussed below.

Figure 5. The test of the different forms of the SER ratios, $D\tau_a/T$, $D{\cdot}\tau_a$, and $D\eta/T$, above the melting temperatures. (**a**) The $D\tau_a/T$ is normalized to their lowest values at the highest temperatures for $Ge_2Sb_2Te_5$, Ag-In-Sb-Te, $Ge_{15}Sb_{85}$, and GeTe, respectively. For comparison, all y-axes are plotted on the same scale. All liquid alloys show a clear deviation from constant behavior, indicating the breakdown of the SER. T_m indicates the melting temperature of respective alloys. (**b**) The normalized $D{\cdot}\tau_a$ is compared with the form of $D\tau_a/T$ shown in (a). The breakdown appears at a lower temperature in $Ge_2Sb_2Te_5$. The $D\tau_a$ of AIST and $Ge_{15}Sb_{85}$ appear to reach a plateau at high temperature. GeTe exhibits an even "negative

violation" (a decrease with decreasing temperature). (**c**) The normalized $D\eta/T$ is plotted as a function of temperature, where available viscosity η data[24,54,55] are inserted to replace τ_a. Note that η data of $Ge_{15}Sb_{85}$ are not available in the literature and thus not shown. The larger error bars result from the reported 10% errors from the viscosity data. The same scale on the y-axes are used in $Ge_2Sb_2Te_5$ and GeTe for comparison, while the y-axis for AIST is larger to contain all data points. $D\eta/T$, exhibiting a similar behavior as $D\tau_a/T$, deviates from a constant to some extents for all four alloys above their T_m.

Using experimental viscosity data for $Ge_2Sb_2Te_5$, AIST, and GeTe [24,54,55] (not available for $Ge_{15}Sb_{85}$ yet), the SER in the form of Eq. 7a can also be tested. As shown in Fig.5c, a similar breakdown, as in Fig.5a, is observed for all liquid alloys. In AIST, the normalized $D\eta/T$ increases to ~1.8 at around 850 K while the normalized $D\tau_a/T$ approaches ~1.6 at the same temperature. In $Ge_2Sb_2Te_5$, $D\eta/T$ appears to show a shallower slope than that of $D\tau_a/T$. In GeTe, the increase in $D\eta/T$ is even smaller, which explains why the SER is considered approximately valid above T_m in the molecular dynamic simulations of GeTe[29,30]. The difference between Fig.5a and 4c stems from the different temperature dependence of G_∞ in the different alloys, as discussed in Sec.4.2.

With the same dataset in Fig.5c, we can also calculate the effective hydrodynamic radii r_H using Eq. 1. The resulting r_H is an increasing function of temperature, ranging from 0.3 to 0.8 Å (see Fig. S2). It is clear that these values do not have a physical meaning as the radii of atoms. Hence, using an atomic radius to approximate effective r_H in these atomic systems may overestimate the effective r_H in calculations.

Although the SER was initially derived by combining Einstein's equation of diffusion of small particles with Stokes' equation for drag on particles travelling through a fluid, it has been successfully applied to a broad variety of nanoparticles, macromolecules and proteins[56,57]. On the molecular and atomic level, the SER in the forms of Eq.7a-c has been shown to be valid over a wide temperature range in a vast number of liquids[58–62], where D represents the self-diffusion coefficient. The most well-known condition for the SER to break down is the supercooling of a liquid down to ~$1.2T_g$ to a highly viscous state (e.g. η ~ a few Pa s). Yet, there are some cases of a breakdown occurring at a higher temperature ~$2T_g$ (above T_m) in a high-fluidity regime of picoseconds in relaxation time or ~mPa s in viscosity, for example, in water, and in simulations of silicon and silica above a fragile-strong

transition[63,64], and some metallic glassforming liquids[65–67], whose origins have attracted considerable interests and not been fully understood.

In contrast to common considerations in the literature, liquid PCMs appear to belong to the latter cases. In the TIP5P and ST2 models of water, Shi et al.[52,53] showed that the breakdown of the Stokes-Einstein-Debye relation at ~$2T_g$ can originate from the formation of locally favored structures that have increasingly different activation energies for diffusive (translational) and rotational motions. As the reorientation slows down much faster than diffusion during cooling, the Stokes-Einstein-Debye relation breaks down. This occurred when liquid water enters a two-state regime which is a mix of a fast high-temperature regime and a slow low-temperature regime. The authors further showed that a crossover of the two regimes yields a fragile-strong transition. The similar idea of formation of locally favored structures could be applied to explain the observations in PCMs regardless of different microscopic structure details. Schumacher et al., Zalden et al.[68] and others[24,69], using AIMD simulations, showed that Ge-Sb-Te, AIST, $Ge_{15}Sb_{85}$, and GeTe possess mainly octahedral-like local structures in the liquid above their melting points. During cooling, there is a formation of Peierls-like distortions of octahedral-like local structures, which lowers the system energy and widens the pseudo-band gap. We conjecture that the locally distorted octahedral-like structures formed have different activation energies for diffusive and collective motions, which is analogous to the scenario laid out by Shi et al. to explain the breakdown of SER.

If this is the case, the formation of locally favored structures is consistent with a two-regime scenario[35,52], which may lead to a fragile-strong transition and thermodynamic anomalies[4]. The fragile-strong transition and heat capacity maximum have been suggested in various PCMs below T_m and shown explicitly in $Ge_{15}Te_{85}$ just above T_m[70,71]. The investigated alloys appear to be well in line with the formation of locally favored structures and the two-regime scenario. This can be further supported by the occurrence of metal-semiconductor transitions in PCMs[4,31], which correspond to an opening of pseudo-band gap related to the Peierls-like distortion[68]. The above phenomenology might be, although not necessarily, linked to a liquid-liquid transition[4,72]. Direct observations of a liquid-liquid transition in the supercooled liquid regime of PCMs is extremely challenging because it is obscured by ultrafast crystallization. Zalden et al.[68], recently succeeded in resolving the structural changes in

supercooled liquid AIST and $Ge_{15}Sb_{85}$ using femtosecond X-ray diffraction. A pump-probe setup enabled measurements on the nanosecond timescale prior to crystallization during fast quenching. Direct evidence for a liquid-liquid structural transition was observed at 660 K for AIST and 610 K for $Ge_{15}Sb_{85}$, which is about 20-30% below T_m. This added a structural transition to the portfolio of anomalies in liquid PCMs. Whether the same structural transition also occurs in $Ge_2Sb_2Te_5$ and GeTe demands further studies.

4.2 Proportionality coefficient of the Maxwell relation

The viscosity η is a macroscopic quantity that can be linked to the time of stress relaxation in the viscoelastic model of Maxwell (Eq. 2). It is reasonable to treat the timescale of stress relaxation the same as structural relaxation τ_a. On the one hand, the τ_a measured by QENS corresponds to the timescale of collective atomic motions in relaxation processes. On the other hand, viscosity reflects the collective response of atoms to external shearing. The proportionality between η and τ_a has been experimentally tested and verified for various glass-forming melts[67,73]. However, it is not trivial to ask how well the proportionality holds for PCMs and to determine the values of G_∞ in Eq. 2 in the liquid state.

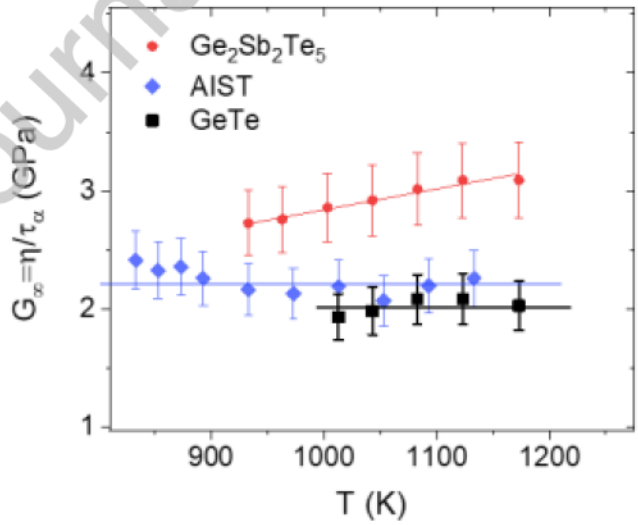

Figure 6. The instantaneous shear modulus $G_\infty = \eta / \tau_a$ from the experimental τ_a and η. While G_∞ of AIST is an approximately temperature-independent constant, the G_∞ values of $Ge_2Sb_2Te_5$ show an increase with increasing temperature. The G_∞ values of GeTe, on the contrary, are approximately constant.

In Figure 6, the proportionality coefficients G_∞ are determined using the measured τ_a and available η from literature[24,54] in the same temperature range. The ratio of η to τ_a, i.e. $G_\infty = \eta / \tau_a$ is shown as a function of temperature for $Ge_2Sb_2Te_5$, AIST, and GeTe in their equilibrium melts. While a nearly constant G_∞ =2.25 GPa is observed for AIST over ~300 K, the values of G_∞ of $Ge_2Sb_2Te_5$, show a mild temperature dependence (~10%), with changes from 2.8 GPa at around 930 K to 3.1 GPa at around 1200 K. The values are somewhat lower than G_∞=3.4 GPa of $Ge_2Sb_2Te_5$ determined by Flores-Ruiz and Micoulaut in their AIMD simulation studies[26]. The G_∞ value of GeTe is approximately a constant of ~2 GPa, which is slightly lower than that of AIST. A larger G_∞ for $Ge_2Sb_2Te_5$ than the other two indicates that more forces (stresses) are required to shear the object, namely, more difficulties for the liquid to flow. The energy barriers for the activated processes of viscous flow are relatively higher in $Ge_2Sb_2Te_5$. For comparison, the G_∞ value in a bulk metallic glassforming viscous melt above T_m between 1060 K and 1255 K is reported as 5.57 GPa for $Zr_{46.25}Ti_{8.25}Cu_{7.5}Ni_{10}Be_{27.5}$[38] using QENS. Although G_∞ of some covalent network glass formers were studied near their T_g using ultrasonic shear wave measurements[74], there are few studies of G_∞ at high temperatures near T_m, because of the difficulty to perform acoustic measurements at a much higher wave frequencies than the relaxation frequency of the liquid.

As shown in Fig. 6, the proportionality between τ_a and η can be regarded as a good approximation in PCMs, which explains why the tests of the SER using the form with τ_a or η gives qualitatively the same results [Figure 5a vs 5c]. While η is a macroscopic quantity measured at a long wave-length $\lambda = 2\pi/q \rightarrow \infty$, τ_a was measured at the first structure factor maximum, q_0, by neutron scattering. Their nearly identical temperature-dependence suggests that the macroscopic viscosity has a microscopic origin. Furukawa and Tanaka[75,76], using molecular dynamics (MD) simulations, showed that the dynamic slowdown of viscosity is directly linked to increasing dynamic heterogeneity. The increased viscosity involves particle rearrangement over a length-scale of ξ and a time comparable to the α-relaxation time τ_α. This implies

that in our cases, there is likely an increasing presence of dynamic heterogeneity with decreasing temperature even above T_m. We speculate that the underlying mechanism governing the dynamic heterogeneity is likely the formation of locally favored structures, as discussed in Sec.4.1. The instantaneous shear modulus G_∞ in Eq. (2) is the high-frequency shear modulus measured on a very short timescale with respect to τ_α. It is the "plateau" shear modulus (denoted as G_0 in Ref.[75]) that can be obtained in simulations by fitting the stress autocorrelation function $G(t) \sim \langle\sigma_{xy}(t)\sigma_{xy}(0)\rangle/VT$, where σ_{xy} is the xy component of the stress tensor[75]. A fit to the plateau and long-time behavior of $\langle\sigma_{xy}(t)\sigma_{xy}(0)\rangle/(VT)$ by the Kohlrausch-Williams-Watts (KWW)-form, $G_\infty exp[-(t/\tau_\alpha)]^\Psi$, yields a pre-exponent G_∞ (or G_0 in Ref.[75]) at $t = 0$. While G_∞ is reported approximately constant[38,77] or decreasing with increasing temperature near T_g in many systems[78], an increase of G_∞ with temperature like that of $Ge_2Sb_2Te_5$ is not uncommon as observed in Lennard-Jones-like systems[79][35]. In the latter simulations, a less soft (relatively harder) potential leads to higher G_∞. We note that the simulations were performed under constant density (volume) condition, while our experiments were under isobaric conditions.

The structural relaxation time τ_α measured by neutron scattering has been treated interchangeable with stress relaxation time τ_s. The τ_α/τ_s ratio in those model systems under constant density conditions also show a weak temperature dependence, which would affect G_∞ values. Whether τ_α/τ_s has a temperature dependence under isobaric conditions and for our systems is unknown. A direct high-frequency ultrasonic measurement of $G(\omega)$ would be needed to compare with the G_∞-values measured here. However, the ultrasonic measurement frequency should be much higher than the inverse picosecond-relaxation time of the liquid. This is impossible with present equipment, where the measurement frequency falls in the range up to 5-20 MHz[80].

4.3. The fractional SER.

To quantify the breakdown of the SER, we can use the 'fractional' Stokes-Einstein relation (F-SER)[37,49,81] in the form with τ_α/T

$$D \propto (\tau_\alpha/T)^{\xi}, \tag{8a}$$

or with η/T,

$$D \propto (\eta/T)^{-\xi} \tag{8b}$$

or with only τ_a

$$D \propto (\tau_a)^{-\xi} \tag{8c}$$

where the fractional exponent $0<\xi<1$ quantifies the extent of the deviation from the SER. For $\xi=1$, the SER holds, and ξ is less than unity for the breakdown of the SER. Figure 7 shows the plot of *[log(D) vs. log(τ_a/T)]*, in which the slope is equal to the fractional exponent ξ.

For $Ge_2Sb_2Te_5$, an apparent linear fitting in the range of 900-1120 K yields $\xi = 0.63 \pm 0.04$, which is close to that of $GeSb_2Te_4$ (ξ=0.60 for T<1150 K) (ref.[20]). Ediger et al.[16] proposed a relation between the crystal growth kinetic coefficient u_{kin} and viscosity η, i.e. $u_{kin} \propto \eta^{\xi^*}$, where the exponent ξ^* is correlated with liquid fragility. Orava et al.[19] estimated the exponent ξ^*=0.67 for $Ge_2Sb_2Te_5$ from the fragility of the alloy. Though a quantitative relation between ξ^* and ξ has not been established, ξ^*=0.67 from ref. [19] is close to the fractional exponent $\xi = 0.63 \pm 0.04$ obtained from the F-SER. The fractional exponent for GeTe is determined in a limited temperature range from T_m = 997 K to 1100 K, and has a value $\xi = 0.65 \pm 0.03$, similar to that of $Ge_2Sb_2Te_5$.

For AIST, the fractional exponent $\xi = 0.36 \pm 0.04$ is markedly lower than those of $Ge_2Sb_2Te_5$ and GeTe, indicating that the temperature dependence of τ_a decouples from that of D somewhat more in AIST than in Ge-Sb-Te and GeTe alloys. The difference in ξ might originate from chemical stoichiometry and/or (Ag, In)-doping effects in AIST. It is worth considering another Sb-rich alloy $Ge_{15}Sb_{85}$, which also has a relatively small $\xi = 0.46 \pm 0.03$ comparable to AIST. This is hardly a coincidence given that both are Sb-rich alloys. The main contribution to their small ξ is that their

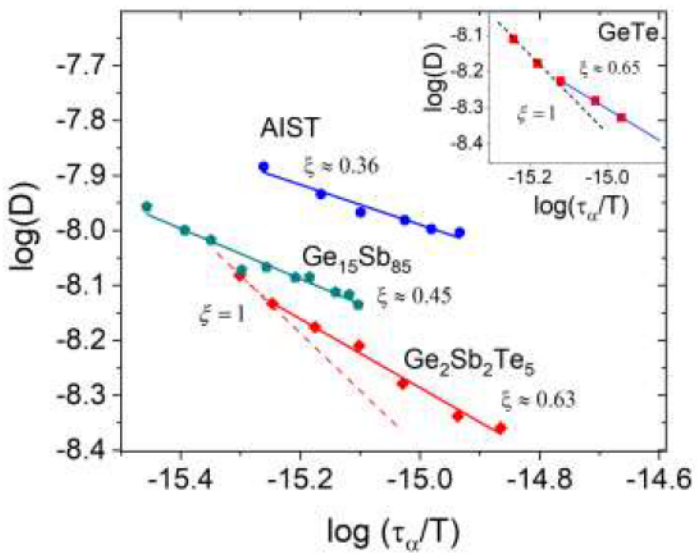

activation energies of diffusivity (~0.11 eV) are less than half of $Ge_2Sb_2Te_5$ (~0.25 eV) and GeTe (~0.32 eV) (see Sec.3.2).

Figure 7. The fractional Stokes-Einstein relation for $Ge_2Sb_2Te_5$, GeTe, AIST, and $Ge_{15}Sb_{85}$. The slope of the *[log(D) vs. log(τ_α/T)]* plot is the fractional exponent ξ. For $Ge_2Sb_2Te_5$, the linear fitting (red line) is limited in the range ≤ 1120 K, where $D\tau_\alpha/T$ deviates from the constant in Fig.5(a-c), and yields $\xi = 0.63 \pm 0.04$, which is comparable to that of $GeSb_2Te_4$ ($\xi = 0.60$) reported earlier. The dashed line indicates the scenario for $\xi = 1$. The data fitting for AIST yields $\xi = 0.36 \pm 0.04$, and for $Ge_{15}Sb_{85}$ yields $\xi = 0.46 \pm 0.03$. Inset: The log-log plot for GeTe. The dashed line indicates a reference slope of ξ=1, whereas the blue solid line is a linear fit from T_m to 1100 K with ξ=0.65 ± 0.03.

Following the similar procedure, we also fitted the data in the plots of *[log(D) vs. log(η/T)], and [log(D) vs. log(τ_α)]*, respectively, to extract the corresponding ξ of Eq. 8b and 8c. The fittings are shown in Figure S3. From $D \propto (\eta/T)^{-\xi}$, we obtained $\xi = 0.73 \pm 0.05$ for $Ge_2Sb_2Te_5$, $\xi = 0.31 \pm 0.03$ for AIST, and $\xi = 0.84 \pm 0.01$ for GeTe. Note that η data of $Ge_{15}Sb_{85}$ are not available. For $D \propto (\tau_\alpha)^{-\xi}$, we have $\xi = 0.79 \pm 0.05$ for $Ge_2Sb_2Te_5$, $\xi = 0.50 \pm 0.06$ for AIST, and $\xi = 0.70 \pm 0.05$ for $Ge_{15}Sb_{85}$. For GeTe, due to the "negative" deviation shown in Fig.5b, the apparent $\xi > 1$ is obtained at the high temperature (T>1100 K) before it decreases to $\xi = 0.79 \pm 0.03$ at lower temperature.

4.4 Implications for the behavior of the supercooled liquid below T_m

The breakdown of the SER in Ge-Sb-Te, AIST, and GeTe alloys occurs in the high-temperature regime above T_m in a high fluidity state, where the structural relaxation is on the timescale of picoseconds. However, the crystallization process during setting of the "on state" which is the rate limiting step in the operation of memory devices, occurs in the supercooled liquid state. It is therefore highly relevant to quantify the liquid dynamics in this temperature range.

An approach to access the dynamics in the supercooled regime is to exploit crystallization rate data in this temperature range. A recent study has derived the diffusivities in supercooled water from the crystal growth velocity of ice in the 'inaccessible' regime (180-262 K) of water[32]. Here we use a similar approach to derive the diffusivity D from experimental $u(T)$ values for supercooled AIST employing the Wilson-Frenkel (W-F) model[32,82],

$$u(T) = [D(T)/\alpha]\left[1 - \exp\left(\frac{-\Delta G(T)}{RT}\right)\right], \quad (9)$$

where ΔG is the Gibbs free energy difference between liquid and crystal, and R is gas constant. The constant α can be determined from a known value of D at a temperature, where u is available.

In the case of AIST, the measured D from QENS can be extrapolated slightly below T_m to overlap

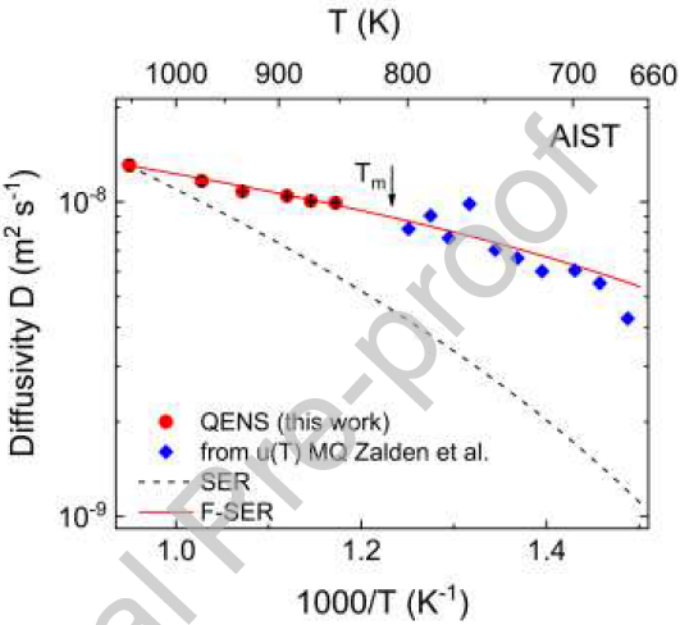

with experimental data of $u(T)$ measured by Zalden et al. using ultrafast femtosecond laser pulses[83]. This permits to determine the value of $\alpha = 1.6\times10^{-11}$ m according to Eq. (9) (see Fig. S4). Then, α is assumed as a temperature-independent constant to calculate $D(T)$ in the supercooled liquid regime from $u(T)$ of melt-quenched AIST[83]. $\Delta G(T)$ is taken from the values derived from heat capacity measurements by Kalb et al.[21]. The resulting diffusivities in the supercooled liquid regime combined with that in the melt for AIST are shown in Fig. 8. A detailed derivation is shown in Fig S4. For $Ge_2Sb_2Te_5$ and GeTe, there are crystal growth velocity data in the supercooled regime, but none near T_m, which does not allow us to determine the α values. Therefore, we have to limit our discussion here only to AIST.

Figure 8. The experimental diffusivities of AIST from QENS (red dots) and the calculated diffusivities from the crystal growth data of melt-quenched samples using the Wilson-Frenkel model

(blue diamonds). The red curve is given by the fractional SER with an exponent $\xi = 0.36$, while the black dashed line is obtained assuming the validity of the SER.

In the regime above ~660 K, the diffusivity is compared to the values from the F-SER (red curve) with the fractional exponent $\xi = 0.36$ (Eq.8a), and those from the SER (black dashed line). The F-SER uses the τ_a values obtained from an extrapolation by a fit with the Vogel-Fulcher-Tammann (VFT) equation, $\tau_a = \tau_0 exp[\mathcal{D}^* T_0/(T-T_0)]$, to the τ_α data measured by QENS above T_m and a data point τ_α=100 s at calorimetric T_g =443 K[84] (which yields τ_0=7.6 × 10^{-14} s, $\mathcal{D}^* \approx 2$ and T_0=420 K). Then, the resulting values of $(\tau_a/T)^{\xi}$ are scaled with a constant to match the experimental value (red dots) at the highest temperature (1053 K), above which we consider the SER to be a reasonable approximation for atomic diffusivity. As such, the absolute D values can be obtained for the F-SER (red curve). Note that the temperature range under discussion is above the reported LLT (T_{LL}=660 K), and therefore corresponds to the fragile liquid state[68]. As shown in Fig. 8, the F-SER (red curve) reproduces the diffusivity data all the way down to about 660 K very well. On the contrary, the SER (black dashed line) predicts much lower diffusivities and exhibits a different curvature. The difference between the F-SER (red) and the SER (dashed) curves develops rapidly with decreasing temperature, and reaches almost one order of magnitude around 660 K. This indicates that the SER breakdown above T_m, extends into the supercool regime and becomes even more pronounced. This implies that the diffusivity decouples from the viscosity. Thus, during cooling from the melt, the diffusivity can maintain high values, even though the viscosity may have already increased. This facilitates the diffusion-controlled nucleation and growth process and is favorable for the fast switching in the supercooled liquid at elevated temperatures.

5. Conclusion

We determine the α-relaxation times and diffusivity of four prominent PCMs $Ge_2Sb_2Te_5$, GeTe, AIST, and $Ge_{15}Sb_{85}$ in the liquid state above T_m using QENS. The Stokes-Einstein relation, frequently used to connect diffusivity and viscosity in liquid PCMs, shows a systematic violation in all alloys above T_m in a high fluidity state. This is likely related to increasing dynamic heterogeneity due to the formation of

locally favored structures such as Peierls-like distortion in liquid PCMs near T_m. This implies that even in the liquid there is evidence for a competition between electron localization and electron delocalization, which also characterizes metavalent bonding in the crystalline state. Further support for this conclusion comes from previous studies which have reported a reentrant Peierls distortion in liquid GeTe[69]. Note that a very recent study suggested that such a competition also exists in amorphous selector materials (e.g. Ge-Se) and plays a key role in the ovonic threshold switching, where the electronic on-state has also been identified as being 'metavalent'[85]. The relation between diffusivity and α-relaxation times (or viscosity) should be described by the F-SER (Eq.8a) with the fractional exponent ξ =0.63 ± 0.04 for $Ge_2Sb_2Te_5$, ξ =0.65 ± 0.03 for GeTe, ξ =0.36 ± 0.04 for AIST, and ξ =0.46 ± 0.03 for $Ge_{15}Sb_{85}$. Furthermore, the absolute values of diffusivity allow to derive the diffusivity from the crystal growth below T_m. The result can be described by the F-SER and shows markedly higher values than those expected from the Stokes-Einstein relation. The already high diffusivity remains high in the fragile liquid and provides a maximum kinetic factor possible for diffusion-controlled nucleation and growth of crystals. This high atomic mobility state is crucial to enable fast switching in PCMs.

Appendix A: Supporting Information

The Supporting Information is available on the publications website.

Figure S1, S2, S3, S4

Table S1: Coherent and incoherent scattering cross sections of elements used in this study. Taken from NIST

Supporting text: Consideration of incoherent and coherent scattering contributions at the low-q range

ACKNOWLEDGMENT

The authors acknowledge the beamtime at the TOFTOF instrument operated by FRM II at the Heinz Maier-Leibnitz Zentrum(MLZ), Garching, Germany. S.W. and C.P. acknowledge financial support provided by FRM II to perform the QENS measurements. S.W. and C.P thank Reiner Zorn for discussion. S.W. acknowledges financial support from the Deutsche Forschungsgemeinschaft (DFG)

(project #:422219280) and Place-to-be RWTH Start-Up fund. M.W. acknowledges financial support from SFB917 of DFG. PL acknowledges financial support from NSF-DMR under grant#: 1832817.

REFERENCES

[1] M. Wuttig, N. Yamada, Phase-change materials for rewriteable data storage., Nat Mater. 6 (2007) 824–32.
[2] H.S.P. Wong, S. Raoux, S. Kim, J. Liang, J.P. Reifenberg, B. Rajendran, M. Asheghi, K.E. Goodson, Phase Change Memory, Proc. IEEE. 98 (2010) 2201–2227.
[3] M. Wuttig, V.L. Deringer, X. Gonze, C. Bichara, J.-Y. Raty, Incipient Metals: Functional Materials with a Unique Bonding Mechanism, Adv. Mater. 30 (2018) 1803777.
[4] S. Wei, P. Lucas, C.A. Angell, Phase-change materials: The view from the liquid phase and the metallicity parameter, MRS Bull. 44 (2019) 691–698.
[5] F. Rao, K. Ding, Y. Zhou, Y. Zheng, M. Xia, S. Lv, Z. Song, S. Feng, I. Ronneberger, R. Mazzarello, W. Zhang, E. Ma, Reducing the stochasticity of crystal nucleation to enable subnanosecond memory writing, Science. (2017) eaao3212.
[6] M. Wuttig, H. Bhaskaran, T. Taubner, Phase-change materials for non-volatile photonic applications, Nat. Photonics. 11 (2017) 465–476.
[7] J.-Y. Raty, M. Schumacher, P. Golub, V.L. Deringer, C. Gatti, M. Wuttig, A Quantum-Mechanical Map for Bonding and Properties in Solids, Adv. Mater. 31 (2019) 1806280.
[8] W. Zhang, R. Mazzarello, M. Wuttig, E. Ma, Designing crystallization in phase-change materials for universal memory and neuro-inspired computing, Nat. Rev. Mater. 4 (2019) 150–168.
[9] L. Hoddeson, P. Garrett, The discovery of Ovshinsky switching and phase-change memory, Phys. Today. 71 (2018) 44–51.
[10] C.D. Wright, Crystal-clear neuronal computing, Nat. Nanotechnol. 11 (2016) 655–656.
[11] K. Shportko, S. Kremers, M. Woda, D. Lencer, J. Robertson, M. Wuttig, Resonant bonding in crystalline phase-change materials, Nat. Mater. 7 (2008) 653–658.
[12] W. Zhang, A. Thiess, P. Zalden, R. Zeller, P.H. Dederichs, J.-Y. Raty, M. Wuttig, S. Blügel, R. Mazzarello, Role of vacancies in metal–insulator transitions of crystalline phase-change materials, Nat. Mater. 11 (2012) 952–956.
[13] M. Zhu, O. Cojocaru-Mirédin, A.M. Mio, J. Keutgen, M. Küpers, Y. Yu, J.-Y. Cho, R. Dronskowski, M. Wuttig, Unique Bond Breaking in Crystalline Phase Change Materials and the Quest for Metavalent Bonding, Adv. Mater. 30 (2018) 1706735.
[14] B.J. Kooi, M. Wuttig, Chalcogenides by Design: Functionality through Metavalent Bonding and Confinement, Adv. Mater. 32 (n.d.) 1908302.
[15] W.H. Zachariasen, The atomic arrangement in glass, J. Am. Chem. Soc. 54 (1932) 3841–3851.
[16] M.D. Ediger, P. Harrowell, L. Yu, Crystal growth kinetics exhibit a fragility-dependent decoupling from viscosity, J. Chem. Phys. 128 (2008) 034709.

[17] W.L. Johnson, J.H. Na, M.D. Demetriou, Quantifying the origin of metallic glass formation, Nat. Commun. 7 (2016) 10313.
[18] M. Salinga, E. Carria, A. Kaldenbach, M. Bornhöfft, J. Benke, J. Mayer, M. Wuttig, Measurement of crystal growth velocity in a melt-quenched phase-change material, Nat. Commun. 4 (2013) 2371.
[19] J. Orava, L. Greer, B. Gholipour, D.W. Hewak, C.E. Smith, Characterization of supercooled liquid Ge2Sb2Te5 and its crystallization by ultrafast-heating calorimetry., Nat. Mater. 11 (2012) 279–83.
[20] S. Wei, Z. Evenson, M. Stolpe, P. Lucas, C.A. Angell, Breakdown of the Stokes-Einstein relation above the melting temperature in a liquid phase-change material, Sci. Adv. 4 (2018) eaat8632.
[21] J. Kalb, F. Spaepen, M. Wuttig, Calorimetric measurements of phase transformations in thin films of amorphous Te alloys used for optical data storage, J. Appl. Phys. 93 (2003) 2389–2393.
[22] J. Pries, S. Wei, M. Wuttig, P. Lucas, Switching between Crystallization from the Glassy and the Undercooled Liquid Phase in Phase Change Material Ge2Sb2Te5, Adv. Mater. 31 (2019) 1900784.
[23] N. Yamada, E. Ohno, K. Nishiuchi, N. Akahira, M. Takao, Rapid-phase transitions of GeTe-Sb2Te3 pseudobinary amorphous thin films for an optical disk memory, J. Appl. Phys. 69 (1991) 2849–2856.
[24] M. Schumacher, H. Weber, P. Jóvári, Y. Tsuchiya, T.G. Youngs, I. Kaban, Riccardo Mazzarello, Structural, electronic and kinetic properties of the phase-change material Ge2Sb2Te5 in the liquid state, Sci. Rep. 6 (2016) 27434.
[25] J. Orava, D.W. Hewak, A.L. Greer, Fragile-to-Strong Crossover in Supercooled Liquid Ag-In-Sb-Te Studied by Ultrafast Calorimetry, Adv. Funct. Mater. 25 (2015) 4851–4858.
[26] H. Flores-Ruiz, M. Micoulaut, From elemental tellurium to Ge2Sb2Te5 melts: High temperature dynamic and relaxation properties in relationship with the possible fragile to strong transition, J. Chem. Phys. 148 (2018) 034502.
[27] M. T. Cicerone, M. D. Ediger, Enhanced translation of probe molecules in supercooled o-terphenyl: Signature of spatially heterogeneous dynamics?, J. Chem. Phys. 104 (1996) 7210–7218.
[28] I. Chang, H. Sillescu, Heterogeneity at the Glass Transition: Translational and Rotational Self-Diffusion, J. Phys. Chem. B. 101 (1997) 8794–8801.
[29] G.C. Sosso, J. Behler, M. Bernasconi, Breakdown of Stokes–Einstein relation in the supercooled liquid state of phase change materials, Phys. Status Solidi B. 249 (2012) 1880–1885.
[30] G.C. Sosso, J. Colombo, J. Behler, E. Del Gado, M. Bernasconi, Dynamical Heterogeneity in the Supercooled Liquid State of the Phase Change Material GeTe, J. Phys. Chem. B. 118 (2014) 13621–13628.
[31] S. Wei, G.J. Coleman, P. Lucas, C.A. Angell, Glass Transitions, Semiconductor-Metal Transitions, and Fragilities in Ge-V-Te (V=As, Sb) Liquid Alloys: The Difference One Element Can Make, Phys. Rev. Appl. 7 (2017) 034035.
[32] Y. Xu, N.G. Petrik, R.S. Smith, B.D. Kay, G.A. Kimmel, Growth rate of crystalline ice and the diffusivity of supercooled water from 126 to 262 K, Proc. Natl. Acad. Sci. 113 (2016) 14921–14925.

[33] W. Zhang, I. Ronneberger, P. Zalden, M. Xu, M. Salinga, M. Wuttig, R. Mazzarello, How fragility makes phase-change data storage robust: insights from ab initio simulations, Sci. Rep. 4 (2014) 6529.
[34] J.C. Maxwell, Philos Trans R Soc Lond. 157 (1867).
[35] Z. Shi, P.G. Debenedetti, F.H. Stillinger, Relaxation processes in liquids: Variations on a theme by Stokes and Einstein, J. Chem. Phys. 138 (2013) 12A526.
[36] S.-H. Chen, F. Mallamace, C.-Y. Mou, M. Broccio, C. Corsaro, A. Faraone, L. Liu, The violation of the Stokes–Einstein relation in supercooled water, Proc. Natl. Acad. Sci. 103 (2006) 12974–12978.
[37] L. Xu, F. Mallamace, Z. Yan, F.W. Starr, S.V. Buldyrev, H. Eugene Stanley, Appearance of a fractional Stokes–Einstein relation in water and a structural interpretation of its onset, Nat. Phys. 5 (2009) 565–569.
[38] F. Yang, T. Unruh, A. Meyer, Coupled relaxation processes in a glass forming ZrTiNiCuBe liquid, EPL Europhys. Lett. 107 (2014) 26001.
[39] F. Yang, T. Kordel, D. Holland-Moritz, T. Unruh, A. Meyer, Structural relaxation as seen by quasielastic neutron scattering on viscous Zr–Ti–Cu–Ni–Be droplets, J. Phys. Condens. Matter. 23 (2011) 254207.
[40] T. Unruh, J. Neuhaus, W. Petry, The high-resolution time-of-flight spectrometer TOFTOF, Nucl. Instrum. Methods Phys. Res. Sect. Accel. Spectrometers Detect. Assoc. Equip. 580 (2007) 1414–1422.
[41] W. Lohstroh, Z. Evenson, TOFTOF: Cold neutron time-of-flight spectrometer, J. Large-Scale Res. Facil. JLSRF. 1 (2015) 15.
[42] O. Arnold, J.C. Bilheux, J.M. Borreguero, A. Buts, S.I. Campbell, L. Chapon, M. Doucet, N. Draper, R. Ferraz Leal, M.A. Gigg, V.E. Lynch, A. Markvardsen, D.J. Mikkelson, R.L. Mikkelson, R. Miller, K. Palmen, P. Parker, G. Passos, T.G. Perring, P.F. Peterson, S. Ren, M.A. Reuter, A.T. Savici, J.W. Taylor, R.J. Taylor, R. Tolchenov, W. Zhou, J. Zikovsky, Mantid—Data analysis and visualization package for neutron scattering and μ SR experiments, Nucl. Instrum. Methods Phys. Res. Sect. Accel. Spectrometers Detect. Assoc. Equip. 764 (2014) 156–166.
[43] A. Meyer, Atomic transport in dense multicomponent metallic liquids, Phys. Rev. B. 66 (2002) 134205.
[44] A. Meyer, The measurement of self-diffusion coefficients in liquid metals with quasielastic neutron scattering, EPJ Web Conf. 83 (2015) 01002.
[45] P. Villars, H. Okamoto, Ge-Sb Binary Phase Diagram 0-100 at.% Sb: Datasheet from "PAULING FILE Multinaries Edition – 2012" in SpringerMaterials (https://materials.springer.com/isp/phase-diagram/docs/c_0901215), Springer-Verlag Berlin Heidelberg & Material Phases Data System (MPDS), Switzerland & National Institute for Materials Science (NIMS), Japan, 2012. https://materials.springer.com/isp/phase-diagram/docs/c_0901215.
[46] P. Villars, H. Okamoto, Ge-Te Binary Phase Diagram 40-61 at.% Te: Datasheet from "PAULING FILE Multinaries Edition – 2012" in SpringerMaterials (https://materials.springer.com/isp/phase-diagram/docs/c_0103374), Springer-Verlag Berlin Heidelberg & Material Phases Data System (MPDS), Switzerland & National Institute for

Materials Science (NIMS), Japan, 2016. https://materials.springer.com/isp/phase-diagram/docs/c_0103374.
[47] J.P. Boon, S. Yip, Molecular Hydrodynamics, Courier Corporation, 1980.
[48] R. Jeyasingh, S.W. Fong, J. Lee, Z. Li, K.-W. Chang, D. Mantegazza, M. Asheghi, K.E. Goodson, H.-S.P. Wong, Ultrafast Characterization of Phase-Change Material Crystallization Properties in the Melt-Quenched Amorphous Phase, Nano Lett. 14 (2014) 3419–3426.
[49] S.R. Becker, P.H. Poole, F.W. Starr, Fractional Stokes-Einstein and Debye-Stokes-Einstein Relations in a Network-Forming Liquid, Phys. Rev. Lett. 97 (2006) 055901.
[50] R. Yamamoto, A. Onuki, Heterogeneous Diffusion in Highly Supercooled Liquids, Phys. Rev. Lett. 81 (1998) 4915–4918.
[51] Y. Jung, J.P. Garrahan, D. Chandler, Excitation lines and the breakdown of Stokes-Einstein relations in supercooled liquids, Phys. Rev. E. 69 (2004) 061205.
[52] R. Shi, J. Russo, H. Tanaka, Origin of the emergent fragile-to-strong transition in supercooled water, Proc. Natl. Acad. Sci. 115 (2018) 9444–9449.
[53] R. Shi, J. Russo, H. Tanaka, Common microscopic structural origin for water's thermodynamic and dynamic anomalies, J. Chem. Phys. 149 (2018) 224502.
[54] J. Orava, H. Weber, I. Kaban, A.L. Greer, Viscosity of liquid Ag–In–Sb–Te: Evidence of a fragile-to-strong crossover, J. Chem. Phys. 144 (2016) 194503.
[55] H. Weber, M. Schumacher, P. Jóvári, Y. Tsuchiya, W. Skrotzki, R. Mazzarello, I. Kaban, Experimental and *ab initio* molecular dynamics study of the structure and physical properties of liquid GeTe, Phys. Rev. B. 96 (2017).
[56] D.H. Kumar, H.E. Patel, V.R.R. Kumar, T. Sundararajan, T. Pradeep, S.K. Das, Model for Heat Conduction in Nanofluids, Phys. Rev. Lett. 93 (2004) 144301.
[57] M.T. Tyn, T.W. Gusek, Prediction of diffusion coefficients of proteins, Biotechnol. Bioeng. 35 (1990) 327–338.
[58] J. Read, K. Mutolo, M. Ervin, W. Behl, J. Wolfenstine, A. Driedger, D. Foster, Oxygen Transport Properties of Organic Electrolytes and Performance of Lithium/Oxygen Battery, J. Electrochem. Soc. 150 (2003) A1351–A1356.
[59] C. Comminges, R. Barhdadi, M. Laurent, M. Troupel, Determination of Viscosity, Ionic Conductivity, and Diffusion Coefficients in Some Binary Systems: Ionic Liquids + Molecular Solvents, J. Chem. Eng. Data. 51 (2006) 680–685.
[60] D.P. Dobson, J.P. Brodholt, L. Vocadlo, W. Crichton, Experimental verification of the Stokes-Einstein relation in liquid Fe—FeS at 5 GPa, Mol. Phys. 99 (2001) 773–777.
[61] A. Bartsch, K. Rätzke, A. Meyer, F. Faupel, Dynamic Arrest in Multicomponent Glass-Forming Alloys, Phys. Rev. Lett. 104 (2010) 195901.
[62] M.K. Mapes, S.F. Swallen, M.D. Ediger, Self-Diffusion of Supercooled o-Terphenyl near the Glass Transition Temperature, J. Phys. Chem. B. 110 (2006) 507–511.
[63] A. Dehaoui, B. Issenmann, F. Caupin, Viscosity of deeply supercooled water and its coupling to molecular diffusion, Proc. Natl. Acad. Sci. 112 (2015) 12020–12025.
[64] J. Geske, B. Drossel, M. Vogel, Fragile-to-strong transition in liquid silica, AIP Adv. 6 (2016) 035131.

[65] A. Jaiswal, T. Egami, Y. Zhang, Atomic-scale dynamics of a model glass-forming metallic liquid: Dynamical crossover, dynamical decoupling, and dynamical clustering, Phys. Rev. B. 91 (2015) 134204.
[66] R. Soklaski, V. Tran, Z. Nussinov, K.F. Kelton, L. Yang, A locally preferred structure characterises all dynamical regimes of a supercooled liquid, Philos. Mag. 96 (2016) 1212–1227.
[67] J. Brillo, A.I. Pommrich, A. Meyer, Relation between Self-Diffusion and Viscosity in Dense Liquids: New Experimental Results from Electrostatic Levitation, Phys. Rev. Lett. 107 (2011) 165902.
[68] P. Zalden, F. Quirin, M. Schumacher, J. Siegel, S. Wei, A. Koc, M. Nicoul, M. Trigo, P. Andreasson, H. Enquist, M.J. Shu, T. Pardini, M. Chollet, D. Zhu, H. Lemke, I. Ronneberger, J. Larsson, A.M. Lindenberg, H.E. Fischer, S. Hau-Riege, D.A. Reis, R. Mazzarello, M. Wuttig, K. Sokolowski-Tinten, Femtosecond x-ray diffraction reveals a liquid–liquid phase transition in phase-change materials, Science. 364 (2019) 1062–1067.
[69] J. Raty, V. Godlevsky, P. Ghosez, C. Bichara, J. Gaspard, J. Chelikowsky, Evidence of a reentrant peierls distortion in liquid GeTe, Phys Rev Lett. 85 (2000) 1950–3.
[70] S. Wei, P. Lucas, C.A. Angell, Phase change alloy viscosities down to Tg using Adam-Gibbs-equation fittings to excess entropy data: A fragile-to-strong transition, J. Appl. Phys. 118 (2015) 034903.
[71] S. Wei, M. Stolpe, O. Gross, W. Hembree, S. Hechler, J. Bednarcik, R. Busch, P. Lucas, Structural evolution on medium-range-order during the fragile-strong transition in Ge15Te85, Acta Mater. 129 (2017) 259–267.
[72] P. Lucas, S. Wei, C.A. Angell, Liquid-liquid phase transitions in glass-forming systems and their implications for memory technology, Int. J. Appl. Glass Sci. 11 (2020) 236–244.
[73] A. Tölle, Neutron scattering studies of the model glass former ortho -terphenyl, Rep. Prog. Phys. 64 (2001) 1473.
[74] S.V. Nemilov, Interrelation between shear modulus and the molecular parameters of viscous flow for glass forming liquids, J. Non-Cryst. Solids. 352 (2006) 2715–2725.
[75] A. Furukawa, H. Tanaka, Direct evidence of heterogeneous mechanical relaxation in supercooled liquids, Phys. Rev. E. 84 (2011) 061503.
[76] A. Furukawa, H. Tanaka, Nonlocal Nature of the Viscous Transport in Supercooled Liquids: Complex Fluid Approach to Supercooled Liquids, Phys. Rev. Lett. 103 (2009) 135703.
[77] I. Fuereder, P. Ilg, Influence of inherent structure shear stress of supercooled liquids on their shear moduli, J. Chem. Phys. 142 (2015) 144505.
[78] W.L. Johnson, M.D. Demetriou, J.S. Harmon, M.L. Lind, K. Samwer, Rheology and Ultrasonic Properties of Metallic Glass-Forming Liquids: A Potential Energy Landscape Perspective, MRS Bull. 32 (2007) 644–650.
[79] R. Zwanzig, R.D. Mountain, High-Frequency Elastic Moduli of Simple Fluids, J. Chem. Phys. 43 (1965) 4464–4471.
[80] W.H. Wang, The elastic properties, elastic models and elastic perspectives of metallic glasses, Prog. Mater. Sci. 57 (2012) 487–656.
[81] F. Fernandez-Alonso, F.J. Bermejo, S.E. McLain, J.F.C. Turner, J.J. Molaison, K.W. Herwig, Observation of Fractional Stokes-Einstein Behavior in the Simplest Hydrogen-Bonded Liquid, Phys. Rev. Lett. 98 (2007).

[82] K.A. Jackson, Kinetic Processes: Crystal Growth, Diffusion, and Phase Transformations in Materials, John Wiley & Sons, 2006.
[83] P. Zalden, A. von Hoegen, P. Landreman, M. Wuttig, A.M. Lindenberg, How Supercooled Liquid Phase-Change Materials Crystallize: Snapshots after Femtosecond Optical Excitation, Chem. Mater. 27 (2015) 5641–5646.
[84] J.A. Kalb, M. Wuttig, F. Spaepen, Calorimetric measurements of structural relaxation and glass transition temperatures in sputtered films of amorphous Te alloys used for phase change recording, J. Mater. Res. 22 (2007) 748–754.
[85] P. Noé, A. Verdy, F. d'Acapito, J.-B. Dory, M. Bernard, G. Navarro, J.-B. Jager, J. Gaudin, J.-Y. Raty, Toward ultimate nonvolatile resistive memories: The mechanism behind ovonic threshold switching revealed, Sci. Adv. 6 (2020) eaay2830.

Declaration of interests

☒ The authors declare that they have no known competing financial interests or personal relationships that could have appeared to influence the work reported in this paper.

☐The authors declare the following financial interests/personal relationships which may be considered as potential competing interests:

Graphical abstract